Urban Modification of Thunderstorms: An Observational Storm Climatology and Model Case Study for the Indianapolis Urban Region*

DEV NIYOGI,[+] PATRICK PYLE,[+,#] MING LEI,[+] S. PAL ARYA,[#] CHANDRA M. KISHTAWAL,[+,@] MARSHALL SHEPHERD,[&] FEI CHEN,[**] AND BRIAN WOLFE[+]

[+] *Purdue University, West Lafayette, Indiana*
[#] *Department of Marine, Earth, and Atmospheric Sciences, North Carolina State University, Raleigh, North Carolina*
[@] *Space Applications Center, Indian Space Research Organization, Ahmadabad, India*
[&] *Department of Geography, University of Georgia, Athens, Georgia*
[**] *National Center of Atmospheric Research,[++] Boulder, Colorado*

(Manuscript received 24 July 2007, in final form 16 August 2010)

ABSTRACT

A radar-based climatology of 91 unique summertime (May 2000–August 2009) thunderstorm cases was examined over the Indianapolis, Indiana, urban area. The study hypothesis is that urban regions alter the intensity and composition/structure of approaching thunderstorms because of land surface heterogeneity. Storm characteristics were studied over the Indianapolis region and four peripheral rural counties approximately 120 km away from the urban center. Using radar imagery, the time of event, changes in storm structure (splitting, initiation, intensification, and dissipation), synoptic setting, orientation, and motion were studied. It was found that more than 60% of storms changed structure over the Indianapolis area as compared with only 25% over the rural regions. Furthermore, daytime convection was most likely to be affected, with 71% of storms changing structure as compared with only 42% at night. Analysis of radar imagery indicated that storms split closer to the upwind urban region and merge again downwind. Thus, a larger portion of small storms (50–200 km^2) and large storms (>1500 km^2) were found downwind of the urban region, whereas midsized storms (200–1500 km) dominated the upwind region. A case study of a typical storm on 13 June 2005 was examined using available observations and the fifth-generation Pennsylvania State University–NCAR Mesoscale Model (MM5), version 3.7.2. Two simulations were performed with and without the urban land use/Indianapolis region in the fourth domain (1.33-km resolution). The storm of interest could not be simulated without the urban area. Results indicate that removing the Indianapolis urban region caused distinct differences in the regional convergence and convection as well as in simulated base reflectivity, surface energy balance (through sensible heat flux, latent heat flux, and virtual potential temperature changes), and boundary layer structure. Study results indicate that the urban area has a strong climatological influence on regional thunderstorms.

1. Introduction

Land use/land cover (LULC) change and resulting urbanization can affect regional weather and climate (Pielke and Niyogi 2009). Heterogeneities in land surface characteristics such as urban–rural interfaces tend to form mesoscale boundaries that can often be conducive to convective initiation or enhancement of preconvection (Changnon 1981; Holt et al. 2006). The change in natural landscape in urban areas can cause changes in temperature (Hafner and Kidder 1999; Zhou and Shepherd 2009), mesoscale convection (Niyogi et al. 2006; Thompson et al. 2007; Miao and Chen 2008), and precipitation amounts (Jauregui and Romales 1996; Bornstein and Lin 2000; Shepherd and Burian 2003; Mote et al. 2007; Rose et al. 2008; Shem and Shepherd 2009; Hand and Shepherd 2009; Bentley et al. 2010; Zhang et al. 2009; Shepherd et al. 2010; M. Lei and D. Niyogi 2010, unpublished manuscript) and can alter regional climate (Oke 1988) by changing regional temperatures (Zhou et al. 2004; Fall et al. 2009) as well as heavy-rainfall trends (Kishtawal et al. 2010).

* Supplemental material related to this paper is available at the Journals Online Web site: http://dx.doi.org/10.1175/2010JAMC1836.s1.

[++] The National Center for Atmospheric Research is sponsored by the National Science Foundation.

Corresponding author address: Dr. Dev Niyogi, Dept. of Agronomy and Dept. of Earth and Atmospheric Sciences, Purdue University, 915 W. State St., West Lafayette, IN 47907.
E-mail: climate@purdue.edu

DOI: 10.1175/2010JAMC1836.1

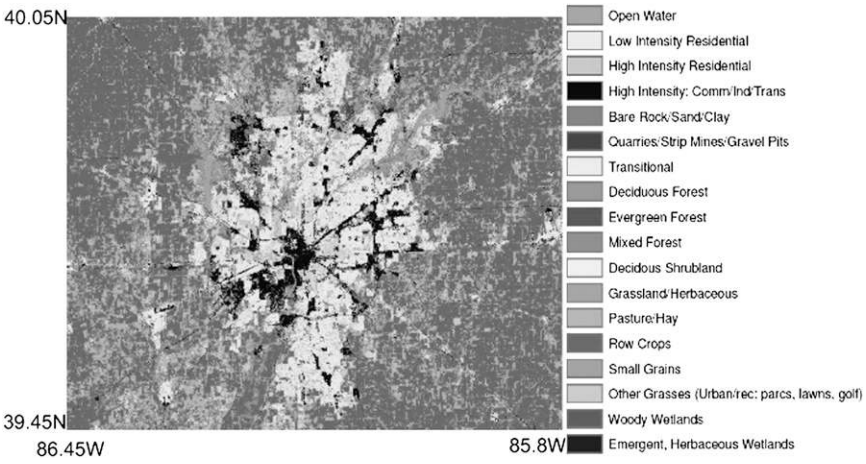

FIG. 1. LULC map generated by Landsat. The Indianapolis urban region is denoted by the lighter shading. The darker peripheral areas represent the agricultural land.

Built-up areas within urban regions store more heat than does the surrounding rural terrain. This energy storage leads to a varying diurnal temperature gradient across the urban–rural interface and an urban heat island (UHI) that can create its own mesoscale convergence. The temperature/heat island effects of urbanization are well known, but the dynamical aspects related to convection and precipitation changes continue to be a topic of active research. Early investigations (Changnon 1968; Landsberg 1970; Huff and Changnon 1972) noted evidence of warm-season rainfall increases of 9%–17% downwind of major cities. The Metropolitan Meteorological Experiment (METROMEX) was a landmark study that took place in the 1970s in the United States (Changnon et al. 1991; Huff 1986) to further investigate modification of rainfall by the urban environment. Results from METROMEX suggest that the urban effects lead to 5%–25% increased precipitation—in particular, 50–75 km downwind of the urban center during the summer months (Changnon et al. 1991; Braham 1981; Shepherd et al. 2002; M. Lei and D. Niyogi 2010, unpublished manuscript). Studies have also shown that urban regions can act to initiate, enhance, or disrupt ongoing convection (Huff and Changnon 1972; Gero et al. 2006; Niyogi et al. 2006; Lei et al. 2008; Miao and Chen 2008; Shem and Shepherd 2009; Zhang et al. 2009). Studies such as Hjelmfelt (1982), Gero and Pitman (2006), and Ikebuchi et al. (2007) showed that the distribution of urban area and anthropogenic heating could greatly influence the distribution and amount of regional rainfall. Studies summarized in Cotton and Pielke (2007, chapter 4) indicate that urban morphological parameters can affect the precipitation variability around urban areas.

A majority of urban precipitation studies have involved one or two event analyses (e.g., Rozoff et al. 2003; Shem and Shepherd 2009; Zhang et al. 2009). To understand the impact of urban area on thunderstorms, this study considered a 10-yr "climatology" of summertime thunderstorms to capture varying storm events that were initiated and maintained under varying synoptic forcing conditions around the urban landscape. Section 2 provides an overview of the Indianapolis urban region and section 3 summarizes the data and methods. Sections 4 and 5 present the results, discussion, and conclusions.

2. Study area: Indianapolis urban region

Indianapolis is located in central Indiana at 39.79°N, 86.15°W. According to the 2000 census from the U.S. Census Bureau (http://www.census.gov/), the city's population has nearly doubled since 1950 and has increased since 1990 from 741 952 to 781 870—an increase of approximately 40 000. Similar to other urban regions, Indianapolis continues to urbanize by transforming open agricultural land to urbanized landscapes. The Indianapolis region is approximately 936 km^2 in size, making the city the twelfth largest in the United States, and was selected for this study for a number of reasons. These include a sharp contrast in LULC from row crops to urban land across a small distance with little to no topography changes (Fig. 1), a familiarity with the regional landscape and meteorological behavior, an existing cooperative relationship with the local National Weather Service forecast office, and the importance of storm-based precipitation to the region's agriculture and economy.

Figure 2 shows a 30-yr average summer precipitation distribution for the Indianapolis urban region. This analysis was developed using North American Regional Reanalysis dataset and available surface stations (S. Fall,

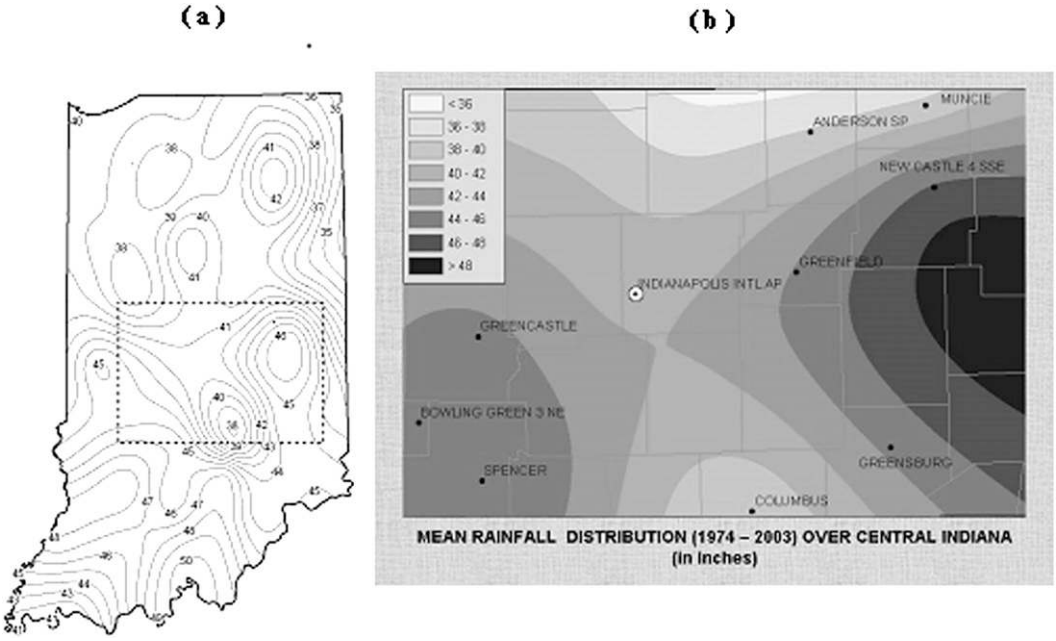

FIG. 2. The 30-yr annual average precipitation distribution (a) over Indiana and (b) around the central Indiana/Indianapolis urban region. The Indianapolis urban region is denoted by the white circle.

Indiana State Climate Office, 2008, personal communication; Oliver 2009). The maximum amount of observed precipitation, in agreement with the findings of urban meteorological studies cited earlier (cf. Braham 1981; Shepherd et al. 2002; Mote et al. 2007; Bentley et al. 2010), is located downwind (east) and southwest of the Indianapolis urban region.

3. Methods

a. Observational analysis

A storm climatological assessment was performed for the Indianapolis urban region for the time period of May 2000–August 2009, focusing on the summer months of May–August for each year. Each event was identified by studying the Storm Prediction Center data archive of severe-weather events (http://www.spc.noaa.gov/exper/archive/events/). Reports of storms from the near-Indianapolis urban region were selected, and 91 thunderstorm cases were available. Storms entered and passed through the urban region. The observed base-reflectivity radar plots were subjectively analyzed for storm-structure changes. Storm-composition change was noted when the change occurred (initiated, split, intensified, or dissipated) in or around the urban or rural region. A summary of the storms and their possible urban impact is available in the table provided as an electronic supplement to this article (http://dx.doi.org/10.1175/2010JAMC1836.s1). To eliminate base-reflectivity biases and improve the diagnosis of a storm or storm complex, different tilts of the radar scan were utilized to better understand storm-composition change and evolution. To test the hypothesis that urban regions alter thunderstorm characteristics, storm-composition change in four surrounding rural regions: north, east, south, and west of Indianapolis within a 120-km radius, was examined (Fig. 3). A distance of 120 km was chosen so as to be sufficiently beyond 2 times the footprint of the urban region and thus to avoid any explicit urban influence. The nearby rural counties examined were Miami (north), Wayne (east), Jackson (south), and Vigo (west). The number of rural cases in each location varied because the composition, alignment, and/or storm motion of each convective case that passes over the urban region may lead to it not passing through a rural region.

b. Modeling analysis

To test further the hypothesis about the impact of the Indianapolis urban area on regional thunderstorms, a model-based sensitivity study was conducted that corresponded to an isolated convective case on 13 June 2005. Available upper-air and surface observational datasets from several surrounding rural upper-air locations and the urban Indianapolis airport were used to assess prestorm environment characteristics. This event was considered to be a typical case and was not selected because of any other special considerations.

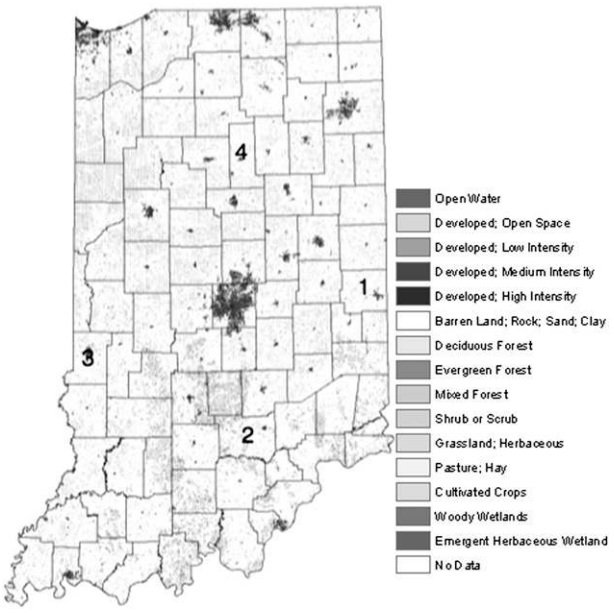

FIG. 3. Indiana GIS county land use map. Numbers indicate the counties used in comparing urban Indianapolis (center) with rural regions: 1—Wayne, 2—Jackson, 3—Vigo, and 4—Miami.

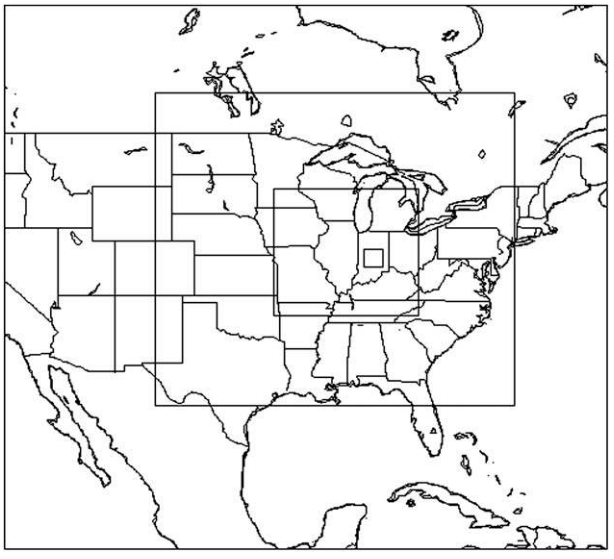

FIG. 4. Map showing the four MM5 nested domains: nest 1 (36 km), nest 2 (12 km), nest 3 (4 km), and nest 4 (1.33 km).

The fifth-generation Pennsylvania State University–National Center for Atmospheric Research Mesoscale Model (MM5) was configured with four 2-way interactive nests with 36- (121 × 91 grid points covering most of the continental United States), 12- (202 × 181 grid points), 4- (244 × 247 grid points), and 1.33-km (100 × 100 grid points) grid spacing. The innermost domain was centered over the Indianapolis urban region (Fig. 4). The model has 45 vertical levels, with higher resolution in the lower levels to accommodate a detailed boundary layer representation. The planetary boundary layer was represented by the Medium-Range Forecasting scheme. Moist processes in the 36- and 12-km nests were simulated using the updated Kain and Fritsch 2 (Kain 2004) cumulus parameterization, with convection explicitly resolved on the finer 4- and 1.33-km nests. Microphysics processes were simulated using the mixed-phase Reisner 1 scheme (Reisner et al. 1998). The ''Noah'' land surface model was used to provide prognostic surface boundary conditions (Chen and Dudhia 2001). It uses the following parameter values to represent zero-order effects of urban surfaces (Liu et al. 2006): 1) roughness length of 0.8 m to represent turbulence generated by roughness elements and drag due to buildings, 2) surface albedo of 0.15 to represent shortwave radiation trapping in urban canyons, 3) volumetric heat capacity of 3.0 $J\ m^{-3}\ K^{-1}$ for urban surfaces (walls, roofs, and roads: assumed as concrete or asphalt), 4) soil thermal conductivity of 3.24 $W\ m^{-1}\ K^{-1}$ to represent the large heat storage in urban buildings and roads, and 5) reduced green-vegetation fraction over urban areas to decrease evaporation. This approach has been successfully employed in real-time weather forecasts (Liu et al. 2006) and to study the impact of urbanization on land–sea breeze circulations (Lo et al. 2007).

The model was initialized using the National Centers for Environmental Prediction Final Model (FNL) 1°-resolution data at 1200 UTC 13 June. In Noah, the urban land surface was represented as an area of decreased albedo and moisture availability with an increase in surface roughness length. To assess the impact of the urban area on the thunderstorm, the model was run with (CONTROL) and without (NOURBAN) the Indianapolis urban area data.

4. Results and discussions

In this section, first the observational summary of the 91 storm events is presented. Then follows the analysis of the modeling case study.

a. Storm climatology

A summary was generated from subjective visualization of the radar base-reflectivity images to determine, on the basis of subjective criteria, whether the storm changed composition or structure as it passed over the four rural locations and/or Indianapolis. The objective was to test whether each storm changed composition—intensified, split, initiated, or dissipated—as it passed over each locale. If the storm changed its morphology only over Indianapolis and underwent no change over

the rural region, it was considered to be indicative that urban region would be affecting the thunderstorm structure. (An example is shown in Fig. 7 discussed below.) Of the 91 storms occurring over the Indianapolis region, 55 (60%) changed their composition/structure. The total numbers of storm cases in each of the four surrounding rural counties were as follows: Miami: 65, Wayne: 74, Jackson: 51, and Vigo: 64. Among these 254 storms, 64 (~25%) show morphology change over these four rural counties. The difference in the number of storms changing their characteristics after passing each of the rural location versus the urban region was tested for chi-square-based statistical significance.

In general for the Miami and Vigo County locations, the null hypothesis could not be rejected at a 99% confidence interval. The results from the other two locations over Wayne and Jackson counties, however, strongly rejected at a 99% confidence level the null hypothesis that rural- and urban-location storm compositions were the same. Therefore, the conclusion was made that the storm characteristics over the urban region as a whole differed significantly from the storm characteristics over rural Wayne and Jackson counties individually, with a 99% confidence that this occurrence was not random.

Additional analysis of each of the 91 storm events in regard to its orientation, storm motion, environmental synoptic conditions, time of the event, and information on the urban storms (e.g., how the storm changed composition, if at all) was performed. Each storm event was separated into five different synoptic classifications: cold-frontal passage (CF), prefrontal convection (PF), warm-frontal boundary (WF), stationary-frontal boundary (SF), upper-level disturbances/low (UL), and a generic category of mesoscale convective systems (MCS) for storms that could not be classified under any particular subcategory. Note that this characterization was a subjective classification to simply group different storm types. Most of the classifications contained subcategories. The CF classification included all cold-frontal boundaries, mainly convection oriented in a linear fashion. Prefrontal convection included all convection that was associated before a cold-frontal passage. These conditions were most often warm and relatively high shear environments. The convection was scattered, isolated, or oriented in a line. The SF classification contained all stationary-frontal boundaries present near the urban region as well as preexisting surface boundaries that were often analyzed as stationary boundaries. MCS encompassed all mesoscale convective clusters or vortices. The UL contained upper-level disturbances, including vorticity maxima and upper low pressure systems. The number of events corresponding to different conditions were CF: 43, PF: 13, WF: 9, SF: 12, MCS: 8, and UL: 6. Note that classification of these events was done on the basis of a review of the synoptic discussions and weather maps and not simply from the abbreviated (and at times cryptic) summary provided in the table in the electronic supplement (http://dx.doi.org/10.1175/2010JAMC1836.s1). Out of these events, the number of storms that changed composition around the urban region and the respective percentages were CF: 27 (63%), PF: 8 (61%), WF: 4 (44%), SF: 10 (82%), MCS: 3 (38%), and UL: 3 (50%). Results of the observational analysis thus showed that the storms most affected by the urban region were those associated with or located near stationary-frontal boundaries, with preexisting surface boundaries often included. This scenario is consistent with the case-2 storm simulated in Shem and Shepherd (2009) that illustrates how a storm may have been enhanced by Atlanta, Georgia.

Of the 91 cases investigated, 56 occurred during the day and 35 were at night. Of the 56 daytime events, 40 (71%) of the storms changed composition; only 15 (42%) of the nighttime events changed composition. The daytime urban boundary layer was dominated by buoyancy due to daytime heating, and the nighttime environment was dominated by shear. The positive buoyancy within the urban environment during the day appeared to cause more storm-composition change when compared with the sheared environment over the urban region even though, on average, nighttime UHI intensities were greater. Previous studies indicated that the UHI circulation was more clearly observed during the daytime than the nighttime because of the urban–rural pressure gradient and vertical mixing during daytime hours (Loose and Bornstein 1977; Shreffler 1978; Fujibe and Asai 1980; Shepherd and Burian 2003). The boundary layer was also more unstable during daytime hours and was more susceptible to slight convective perturbations.

b. Urban modification of thunderstorms

To highlight further the effect of the Indianapolis urban environment on the thunderstorms, we developed a procedure for image analysis of the radar reflectivity data in the vicinity of the Indianapolis urban area (C. Kishtawal et al. 2010, unpublished manuscript). We used 2553 images of composite reflectivity, obtained from the fast-scanning precipitation mode (one image for every 5 min) that were available for 53 different summer storms that passed over the Indianapolis urban area between the years 2000 and 2007 (Fig. 5a). The spatially resampled composite reflectivity products were available in the form of binary images of size 1000 × 720 pixels,

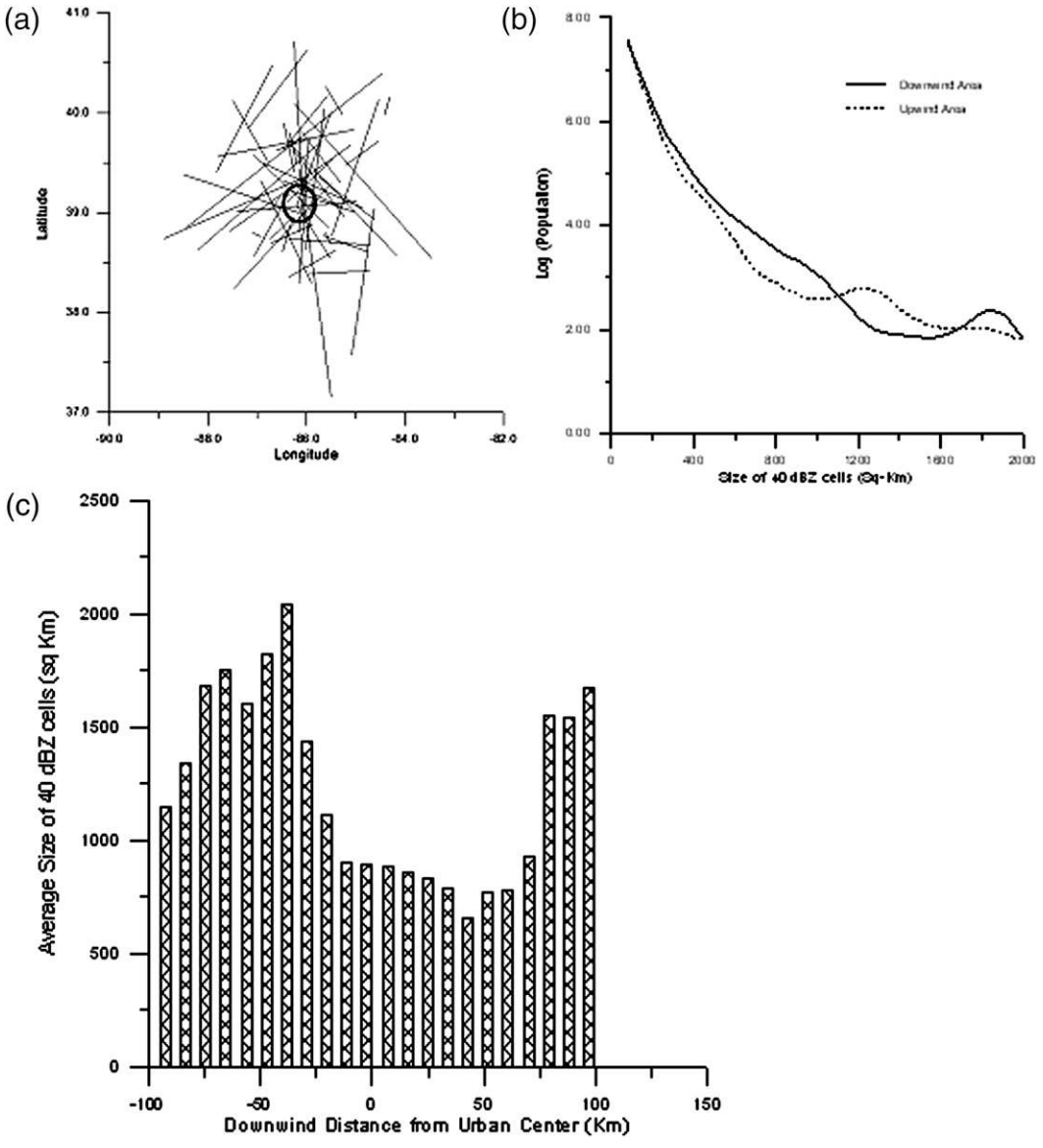

FIG. 5. (a) Storm tracks for the 53 storms. The Indianapolis urban area is indicated by the thick circle. (b) Frequency distribution of high-echo (reflectivity $>$ 40 dBZ) cells of various sizes over the regions downwind (solid line) and upwind (dashed line) of the Indianapolis urban area. The orientation of upwind or downwind area is with respect to individual storm. (c) Variation of the average size of high-echo cells with downwind distance from the Indianapolis urban center.

with each pixel denoting an area of 0.012° $\times$ 0.012°. The mean position (''centroid'') of all radar pixels with reflectivity of l $>$ 40 dBZ (90th percentile of the radar base reflectivity) was considered to be an indicator of storm location in individual radar images (Fig. 5a). The life span of these storms ranged from 2 to 10 h. The composite reflectivity is the maximum reflectivity (measured in reflectivity decibels) from four radar tilt angles (0.5°, 1.45°, 2.40°, and 3.35°) and covers a maximum range of 230 km from the radar location.

For the analysis of the general nature of impact of the urban environment on the storm structure, the upwind and downwind regions were identified in the context of the direction of an individual storm. For this process, every image was rotated by an angle that was equal to the Cartesian angle of the storm track but opposite in sign. This is important, as recent studies have indicated that downwind is relative to the prevailing flow even if a climatologically dominant downwind region exists (Bentley et al. 2010; Rose et al. 2008). Each radar image

was then referenced to a common upwind and downwind region (of 100-km length and 50-km width). The technique of image segmentation and labeling discussed in C. Kishtawal et al. (2010, unpublished manuscript). was used for automated tracking of the high-echo cells in each radar image. Using the 40-dBZ threshold, a ''high-echo cell'' is defined as the entity of ''connected'' radar-image pixels, with each pixel exceeding a base reflectivity of 40 dBZ. Each of the cells detected by this technique was then counted and measured for size. A basic-level analysis revealed significantly more (1.5 times) cells in the downwind region than in the upwind region. This suggests the process of either breakup of incoming large cells into smaller ones or initiation of new cells after the storms cross the urban area. This breakup/splitting or initiation process is supported by Fig. 5b, which shows the frequency distribution of the size of high-echo cells in the downwind and upwind regions. A considerably larger population of smaller cells (size 50–1000 km^2) is obtained in the downwind region. On the other hand, the upwind region shows a larger population of bigger cells (size 1100–1600 km^2). A chi-square test indicates that the difference of two frequency distributions is significant at the 99.9% confidence level, which is sufficient to reject the null hypothesis that the urban environment has no impact on the morphology of storms. The tail side of Fig. 5b indicates a higher population of very large cells (size $>$ 1600 km^2) over the downwind region, which indicates the process of remerging and intensification of the storm cells. Figure 5c provides better insight into the plausible processes of splitting and remerger of these convective cells. The figure shows the variation of the average sizes of high-echo cells at different distances upwind and downwind of the urban center. The high-echo cells begin to grow in size as they approach the urban region. The largest average size of these cells ($\sim$2000 km^2) appears when the storm location is 20 km upwind of the urban region. Beyond this distance, the average size of high-echo cells starts to decrease significantly, possibly because of the process of breaking (or splitting; e.g., Bornstein and Lin 2000). In the downwind region up to a distance of $\sim$40 km from the urban center, the average size of high-echo cells is limited to less than 100 km^2. This figure shows a noticeable change in storm characteristics in the urban vicinity. At a downwind distance beyond 50 km, we note an increase in the size of the high-echo cells. This observation further highlights a process of remerger, or reintensification, of the storm cells. In most of the cases, the growth of the area of the cells is also associated with the intensification of the core of the cells, and the highest values of mean base reflectivity were registered over the downwind region, approximately 50 km away from the urban center. Exactly how the urban environment plays a role in splitting of high-echo storm cells and how the remerger or the intensification of these cells takes place at locations farther downwind is a matter of further investigation and at present is beyond the scope of this study (M. Lei and D. Niyogi 2010, unpublished manuscript).

We also address the issue of the influence of the radar elevation angles on the interpretation of the storm results. By virtue of the radar's angular scanning mechanism, the cells farther from the radar site might have coarser spatial resolution and they may appear as larger in the radar-image analysis procedure. Such artifacts are expected to be symmetric about the radar location and could result in symmetric biases in the upwind and downwind directions. However, we observe an asymmetric behavior both in the population of high-echo cells (with 50% larger counts in upwind region) and in the variation of the average cell size (Fig. 5c) over the upwind and downwind regions. This behavior suggests that the results are not artifacts created by the radar's scanning mechanism. More important, we did not observe significant asymmetries in the crosswind direction (regions perpendicular to the upwind–downwind region) that one would have expected if the radar's scanning mechanism were the sole contributor to the results shown in the previous analysis.

c. *Results of modeling analysis*

Results of the 13 June 2005 storm event using MM5 indicate that convection was initiated following daytime heating (near 29°C or 302 K) and that moderate shear developed well ahead of a potent upper-level low pressure system located in the Great Plains (figure not shown). Storm reports suggest that outflow from another adjacent storm occurring to the storm's northwest could have aided convection. Of interest in the 850-hPa chart was the limited convection across Indiana and the greater convection around the Indianapolis urban region during this time period due to the effects of the short-wave ridge. Figure 6 shows an upper-air sounding from Wilmington, Ohio, (KILN) for 0000 UTC 14 June. Indianapolis does not have upper-air soundings; therefore KILN was selected as the closest upper-air station. Surface winds were out of the southwest at approximately 4–6 m s^{-1} with 0–6-km shear values being moderate at approximately 12 m s^{-1} and a low 3-km storm relative helicity of 73 m^2 s^{-2}. The atmosphere was fairly unstable, with surface-based convective available potential energy values of approximately 1300 J kg^{-1}. The storm was initiated southwest of the urban region and moved quickly northeast. Around 0030 UTC, the storm moved over downtown Indianapolis. The storm

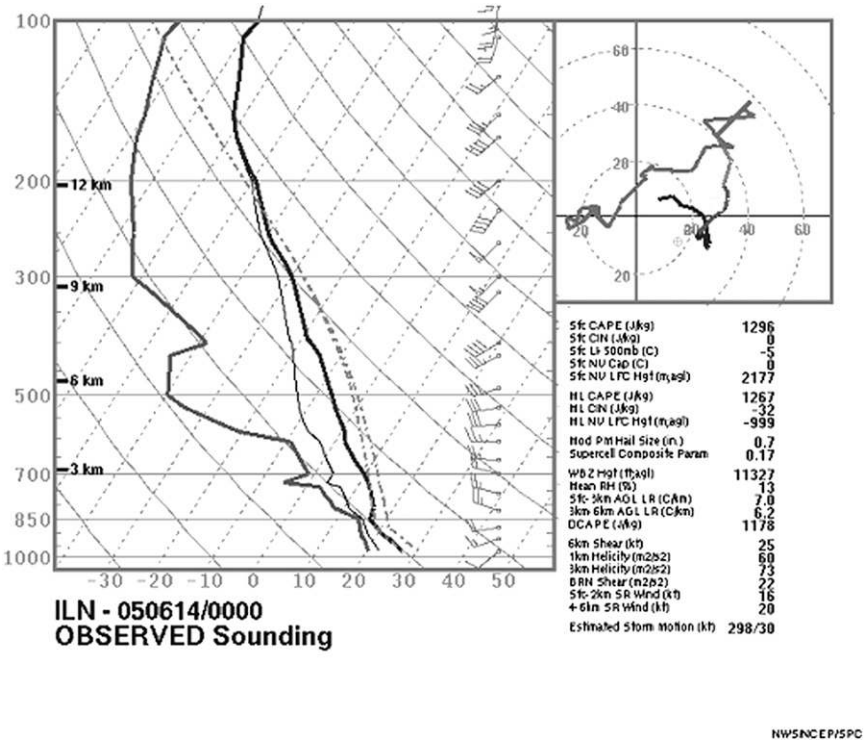

FIG. 6. Wilmington, OH, (KILN) upper-air sounding for 0000 UTC 14 Jun. The image is provided through the courtesy of the National Oceanic and Atmospheric Administration (NOAA) Storm Prediction Center.

then began to intensify [based on an increase in reflectivity and vertically integrated liquid amounts (not shown)] as it moved northeast (downwind) of the urban region. Figure 7 shows a time series of level-II radar images for 0002–0055 UTC 14 June. A single cell is noted at 0002 UTC that, after passing the urban area, shows splitting in the 0042 UTC image and reintensification in the 0055 UTC image. Figure 8 shows that the storm was in the center of the urban region, with the base reflectivity at a 0.5° tilt and the radar reflectivity at a 15.7° tilt, at 0041 UTC. The radar reflectivity increased from 49.5 dBZ at a 0.5° tilt to 69.5 at a 15° tilt spanning approximately 4000 m. This feature shows the elevated reflectivity-decibel core of the convection over the urban region. Past studies have suggested that the increased heating and low-level convergence within the urban environment might aid the storm's updraft speed and thus raise the elevation of the reflectivity core. As the storm moved downwind and northeast of Indianapolis, the core dropped in altitude, and the storm continued into a maximum precipitation region. As the convection moved away from downtown, it began to weaken and break up considerably. Although the storm did not cause any severe weather, Doppler radar estimated over 25 mm of rainfall northeast (downwind) of the city. Two reflectivity cores also showed minor splitting as the storm passed through the downtown area. Because of the moderately sheared environment, the storm splitting might have been caused by storm dynamics; radar velocity analysis (not shown) provides evidence that no rotation occurred with the storm, however. The urbanized land also might have caused the splitting because of the increased friction and drag force associated with buildings, similar to the urban barrier effect mentioned earlier (Bornstein and Lin 2000).

1) MODEL SENSITIVITY ANALYSIS

To test the hypothesis that the changes in the storm characteristics were due to interaction with the urban area, sensitivity tests were run using MM5 with and without the urban area. The urban land use was replaced with the predominant surrounding land use type of ''dryland/cropland and pasture'' with an albedo value of 0.17.

As mentioned earlier, the most significant weather feature for this event was a potent upper-level low in the upper Great Plains region centered near eastern South Dakota. The model reproduced the upper-level feature well, placing it slightly farther southeast, along the Nebraska–South Dakota border. The model also correctly simulated the wind speed and direction as well as

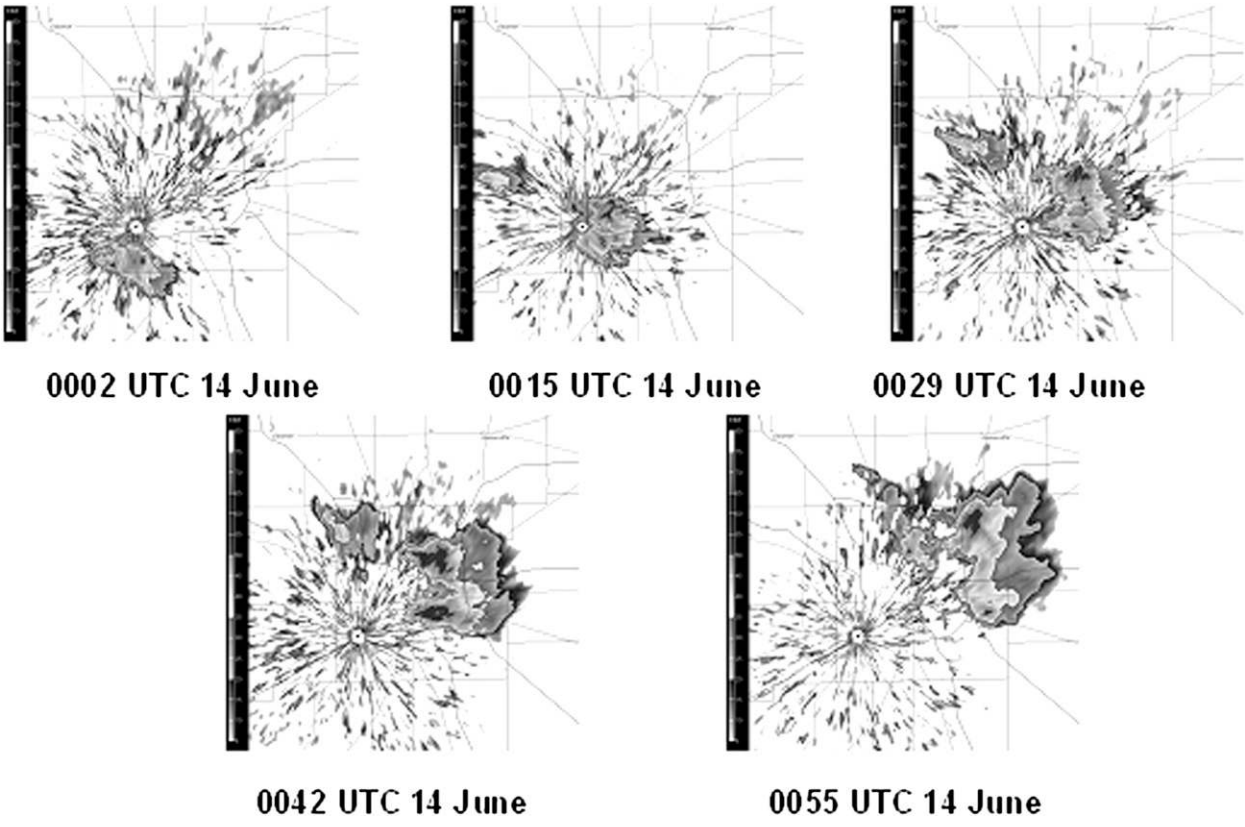

FIG. 7. Level-II base-reflectivity radar plots from Indianapolis for 0002–0055 UTC 14 Jun. The Indianapolis urban region is within the interstate-highway loop just northeast of the radar ''cone of silence.'' Radar data are provided by the National Climatic Data Center.

the surface temperature distribution. Surface temperature fields for nest 3 (4-km grid spacing) at 1800 UTC 13 June (not shown) had temperature values exceeding 303 K near Indianapolis while observations at the Indianapolis International Airport showed a high temperature of 302 K. The airport-based measurements can be expected to be relatively cooler than the downtown region, hence the overestimate was reasonable. The

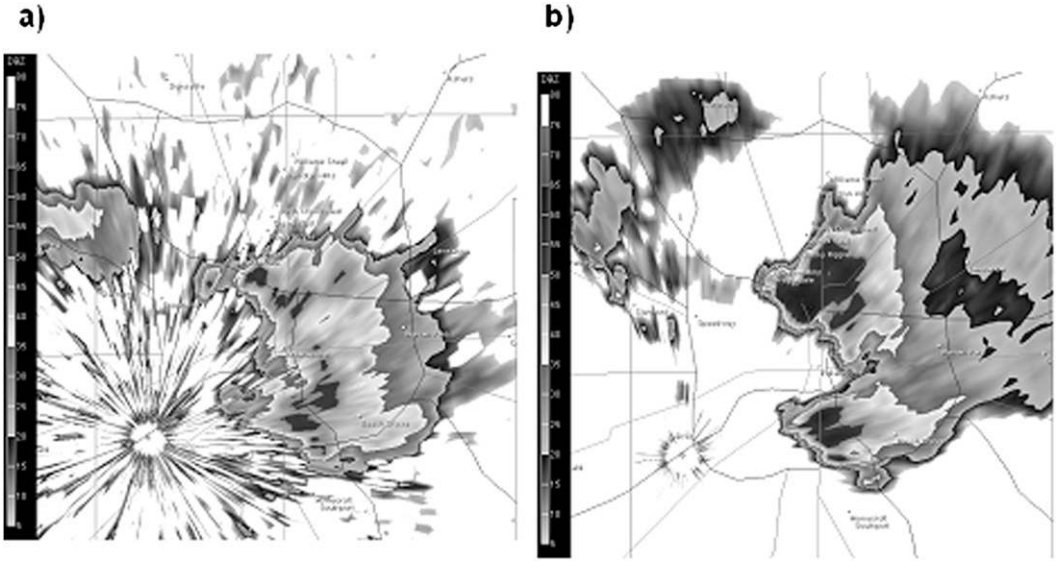

FIG. 8. (a) Indianapolis NWS base reflectivity (0.5° tilt) for 0033 UTC 14 Jun; (b) 15.7° tilt for 0033 UTC 14 Jun.

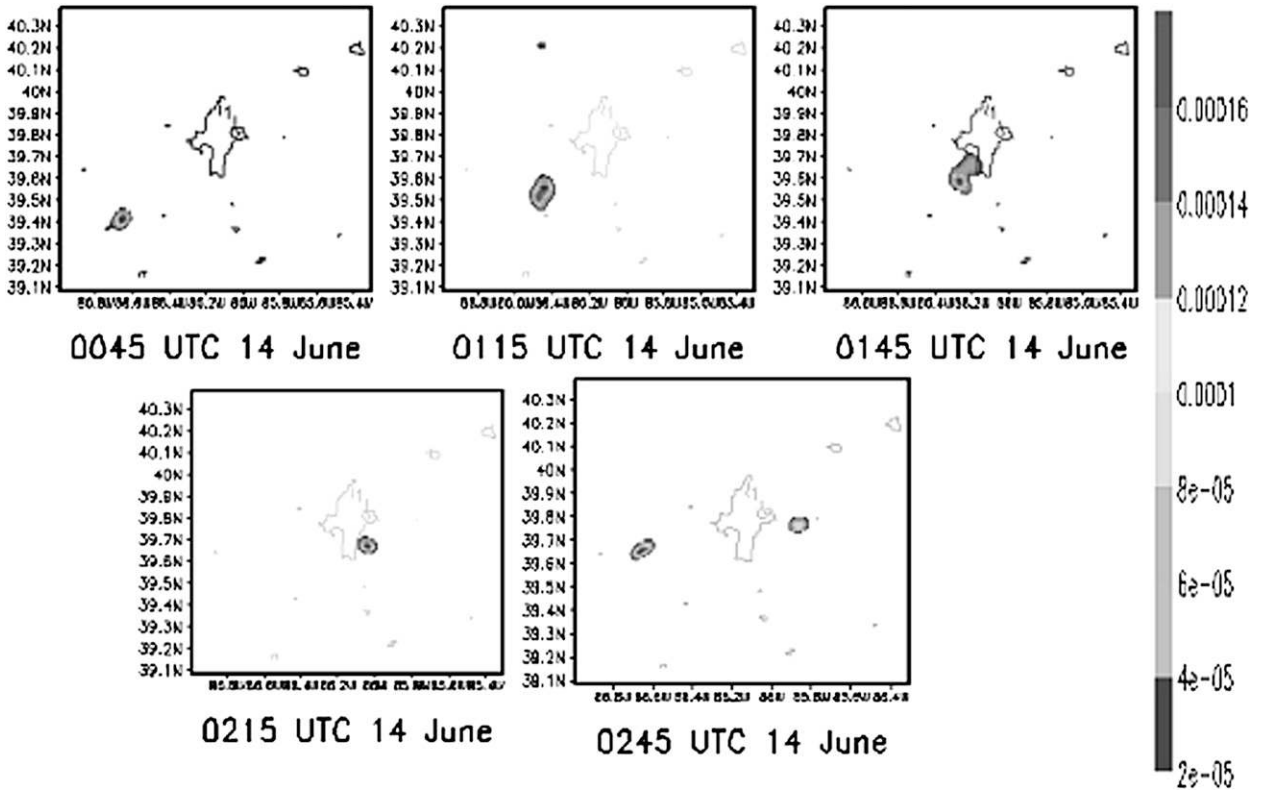

FIG. 9. MM5 CONTROL simulated rainwater (kg kg^{-1}) for 0045–0245 UTC. The Indianapolis urban region is outlined in the center of the domain.

observed base radar reflectivity, shown in Fig. 7, placed the storm over the Indianapolis urban region at 0033 UTC 14 June. The model was slower than the actual storm, however, and the simulated storm did not reach the urban area until 0200 UTC, about 90 min late (Fig. 9). This lateness caused the storm to pass over the urban region at ~1 h after sunset, which reduced the surface fluxes and lead to errors in the simulated storm intensity. Of interest is that the orientation and motion of the storm were fairly well simulated, with the placement slightly farther to the south as compared with the observations. The maximum observed base radar reflectivity appeared over the urban region, with a value of approximately 55 dBZ (Fig. 7) that weakened as the storm moved northeast of the urban region (not shown). The modeled reflectivity was close to that observed, but the maximum value occurred southwest of the urban area. As the storm moved northeastward into the Indianapolis area, it began to weaken in intensity, which was not seen in the observations.

Further investigation of the prestorm environment near Indianapolis revealed an area of convection that was simulated but not observed. The observed and simulated base radar reflectivities show an upper-level low pressure system in the upper Great Plains with a line of convection in the midwestern states. The model correctly simulates the placement of the upper-level low and the convection in Missouri and Michigan but also simulated some spurious convection over Indiana. This spurious convection disrupted the simulation of the UHI and corresponding urban–rural land surface fluxes, which caused the storm to dissipate near the urban region. A number of sensitivity tests with different combinations of the convective parameterization and boundary layer schemes were conducted in an effort to eliminate the prestorm convection; the simulations led to similar results (not shown), however.

In the NOURBAN case, the urban area was replaced with the land use corresponding to the surrounding rural landscapes that possessed different surface properties such as a higher albedo and a lower surface roughness length z_0. Figure 10 shows the NOURBAN simulated base radar reflectivity. Without the urban region, the model, simulating two weak reflectivity cells north and south of the main convection of interest, produces significantly different results. First, the main convection event over central Indiana was not initiated. Urban effects are typically actually observed downwind

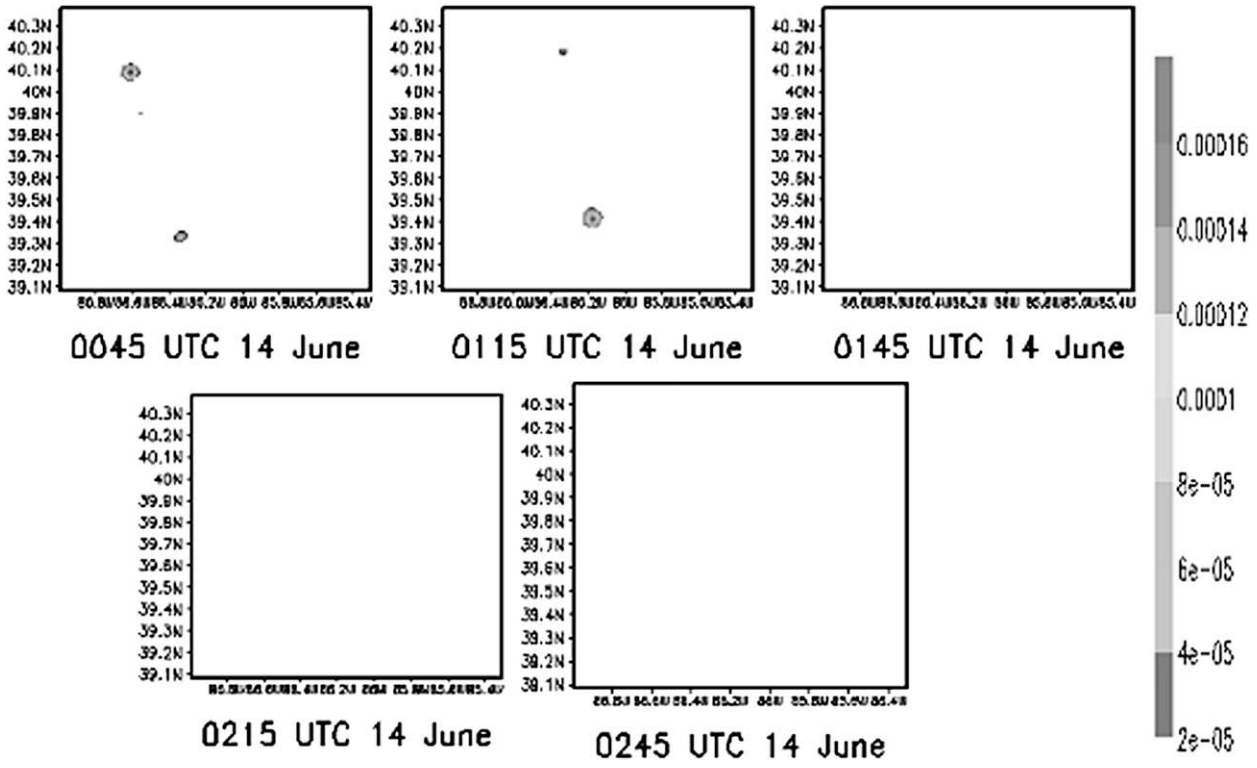

FIG. 10. Model NOURBAN simulated rainwater (kg kg^{-1}) for 0045–0245 UTC. The Indianapolis urban region has been removed and replaced by the dominant (agricultural) surrounding land use category.

of the urban region. Because of the southwesterly flow, these effects normally would be seen northeast of the city; the simulations depicted an effect upstream of the urban region, however. This upwind modification of the storm characteristics was also noted in Lei et al. (2008). Shem and Shepherd (2009) noted that Atlanta creates enhanced convergence at the rural–urban interface. This effect could lead to interactions with the prevailing flow and possible upwind effects as well (Niyogi et al. 2006), but this hypothesis needs further testing.

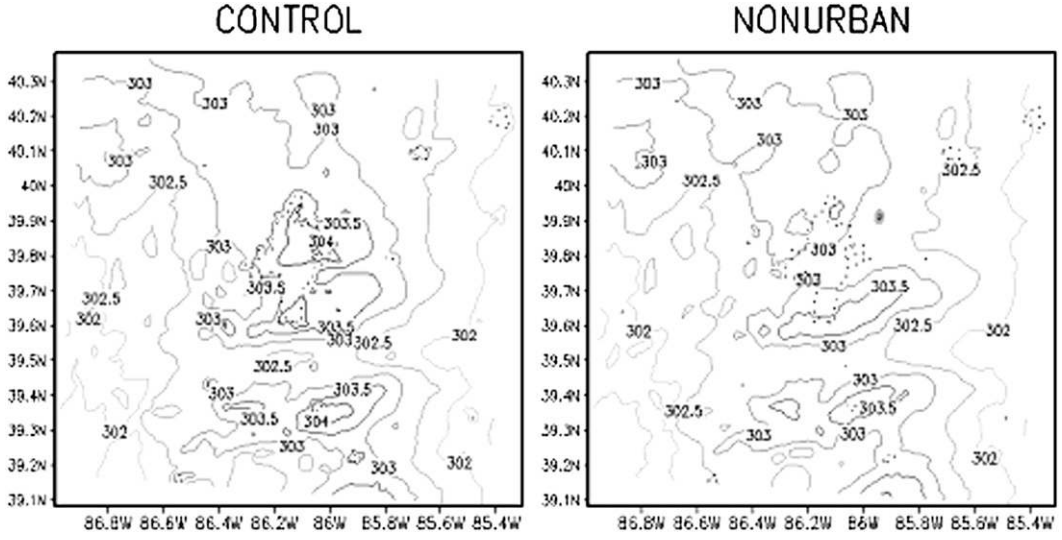

FIG. 11. Nest-4 (1.33 km) 2-m temperature (K) for the (left) CONTROL and (right) NOURBAN simulations for 1800 UTC 13 Jun.

2) Response of prestorm environment/ boundary layer for the CONTROL and NOURBAN cases

Surface energy fluxes are analyzed for domain 4 (1.33-km grid spacing) for two different time periods: 1800 UTC 13 June (pre-''model'' convection) and 0000 UTC 14 June (preconvection initiation of case). The storm was not evident in the simulated base reflectivity until near 0045 UTC. Note that because the model simulated spurious convection, the 1800 UTC plots were intended to provide the ''true'' prestorm environment with and without the urban surface. This provided a time period for examining the boundary layer structure over central Indiana (Indianapolis) for a typical summertime environment near afternoon conditions. The 0000 UTC plots were taken southwest of Indianapolis and showed the PBL before the convection in the CONTROL and NOURBAN simulations, respectively.

Temperature and surface flux plots for 1800 UTC 13 June for both simulations were generated for the prestorm environment. Figure 11 shows the MM5 nest-4 (1.33 km) simulated 2-m temperature plots for the CONTROL and NOURBAN cases. The temperature within the urban area was near 304 K while over the same location the NOURBAN simulation produced temperatures that were approximately 1–2 K cooler. Although the simulated 2-m temperatures were overpredicted when compared with those observed, the larger temperatures in the urban region represented in the CONTROL simulation were advected northeast of Indianapolis. This feature can be attributed to the southwesterly wind flow prevalent in advance of the approaching upper-level low pressure system.

The model-derived temperature/UHI effect was examined in Fig. 12 for the 24-h simulation period. The temperature values were obtained from an average of the values for the urban and rural grid points at each 15-min output interval for the CONTROL simulation. The urban grid points consistently remained 1 K above the rural grid points even during nighttime hours when the UHI is usually larger than the daytime observed values.

Sensible (Hs) and latent (Le) heat flux values are compared between both simulations (figure not shown). As expected, the Hs values were greater and the Le values were smaller for the CONTROL, as compared with the NOURBAN, simulation. The Hs values in the urban region were near 450 W m^{-2} when the urban region was represented, versus 200 W m^{-2} for the NOURBAN case. Similar results were found for the Le flux differences, with the NOURBAN Le values at nearly 400 W m^{-2} more than those in the urban CONTROL case.

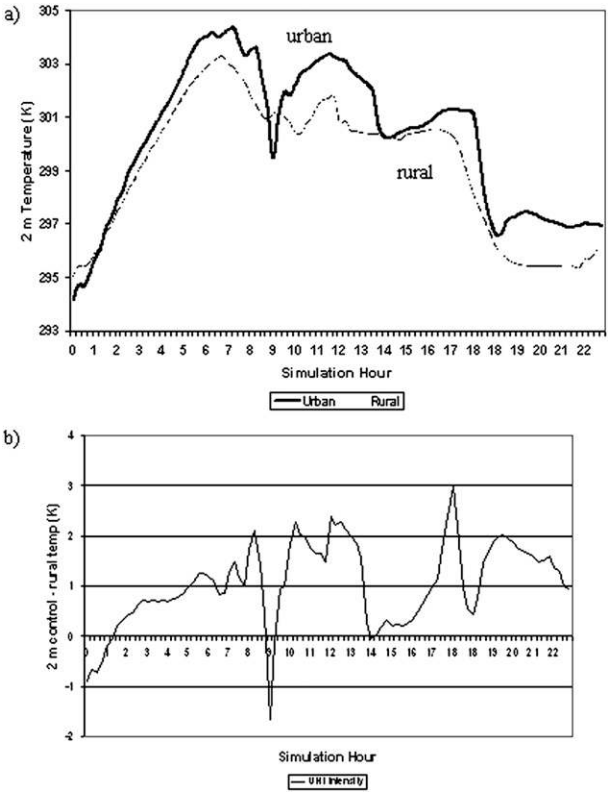

FIG. 12. (a) The 2-m air temperature of urban vs rural grid points through the entire simulation period; (b) corresponding urban − rural differences (UHI intensity).

Vertical 2D plots were analyzed for the rural and urban environments corresponding to the cross section shown in Fig. 13. Cross sections of virtual potential temperature θ_v for both simulations (Figs. 14 and 15) show that θ_v was approximately 1–1.5 K larger near the urban region than in the surrounding rural areas. A UHI signature with a deeper boundary layer (by approximately 200–300 m) in the CONTROL when compared with the NOURBAN case is noted (cf. Rozoff et al. 2003). For optimum UHI circulation patterns to exist, weak surface flow is required. Simulated surface wind speeds were southwesterly on the order of 2–5 m s^{-1}. As seen in Fig. 14, the larger temperatures, driven by the mean surface flow, have been advected toward the northeast urban region. Figure 15 shows the same cross-sectional location for the NOURBAN case. The θ_v values were approximately 1–1.5 K lower throughout the entire cross section when compared with the CONTROL run. Boundary layer heights across the plot were also similar to those found in the rural locations shown in Fig. 14.

Figure 16 shows the vertical velocity (shaded) for the same time period (taken through the C–D cross section in Fig. 13) for both simulations. As expected, the

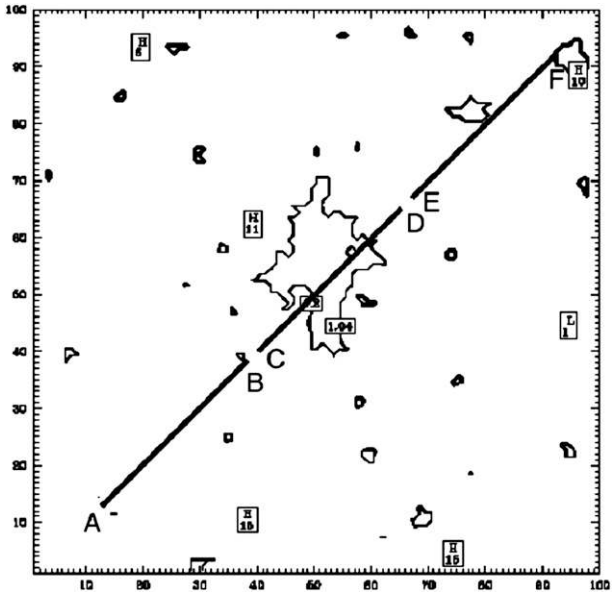

FIG. 13. Cross-sectional locations around the Indianapolis urban region (outlined in the center of the plot).

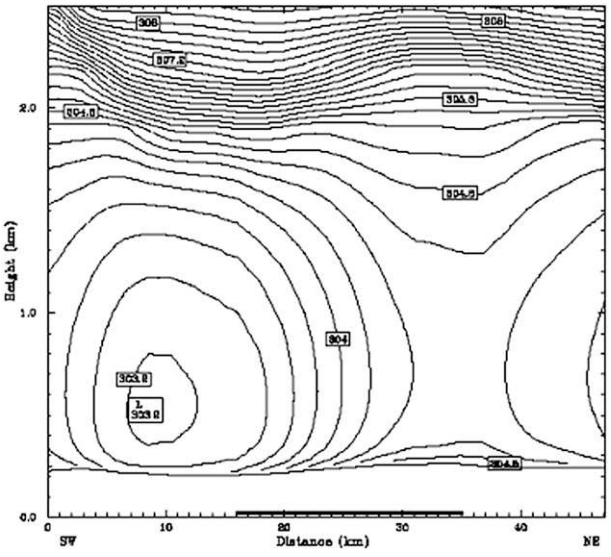

FIG. 14. CONTROL nest-4 (1.33 km) NE–SW cross-sectional plot (0–2.5 km) through Indianapolis for 1800 UTC 13 Jun depicting virtual potential temperature (K). The location of the urban region is outlined in black along the x axis.

differences in θ_v observed in Figs. 14 and 15 are evident in the vertical velocity patterns. The CONTROL simulation shows much stronger vertical velocities in the urban region, with descending air in the rural locations that depicts an urban convergence signature. In conjunction with the lower rural θ_v values, although the NOURBAN case did show large upward motion it also depicted a large area of subsidence that created an environment that inhibited convection. The vertical velocities plotted in Fig. 17 were not strong enough to generate convection; this figure depicts the way an urban region can enhance upward vertical atmospheric motion, however.

d. Convective initiation

Cross-sectional plots of vertical velocity and velocity vectors were analyzed through the A–B line (southwest) of the urban region where the convection was initiated (not shown). We compared plots of vertical velocities (shaded) and velocity vectors for the CONTROL and NOURBAN simulations. Near 0000 UTC, the CONTROL simulated positive vertical velocities of approximately 0.2 m s^{-1} entering the southwest portion of the cross section, whereas the NOURBAN simulation contained areas of negative vertical velocities. As time progresses, however, the vertical velocity fields in the CONTROL simulation continue to propagate and intensify to well above 0.2 m s^{-1} northeastward. A similar pattern was obtained with the NOURBAN simulation; the overall intensities of vertical motion were very small, however, in comparison with the CONTROL. Skew T plots from this region for 0000 UTC (not shown) indicated a lower capping inversion present for the NOURBAN case as well as drier air near 750 hPa. The capping inversion on the CONTROL simulation was near 700 hPa, and the dry layer in the NOURBAN case was not evident for the CONTROL case.

5. Conclusions

Because of the increased urbanization, the effects of urban regions on regional precipitation specifically and on regional weather and climate in general have become an important subject of research. The likely impacts of Indianapolis urban area on central Indiana storm and precipitation characteristics were examined through an observational analysis composed of decadal (2000–2009) radar and synoptic charts for 91 unique thunderstorm cases that occurred near the Indianapolis urban region. The analysis supports the hypothesis that the Indianapolis urban region alters convective thunderstorm characteristics over central Indiana; urban regions more generally can lead to alterations of the precipitation climatology around the urban periphery. Several synoptic categories were chosen to classify each storm event. Stationary frontal boundaries and preexisting surface boundaries along which convection was initiated or propagated appeared to have a storm-composition change rate larger than any other synoptic category. Nearly 60% of the storms changed composition over the urban region as

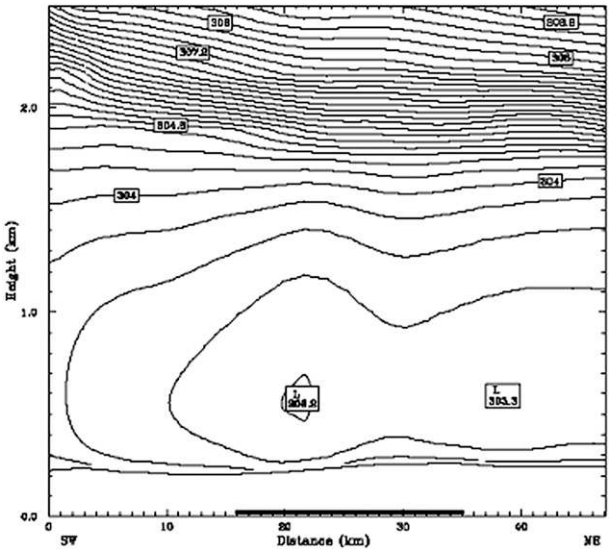

FIG. 15. As in Fig. 14, but for the NOURBAN simulation. Note that the outlined urban region is not represented in the simulation.

compared with 25% over the rural region. Daytime convection changed composition more (71%) as compared with the nocturnal storms (42%). The majority of storm splitting occurred closer to the urban region, and merging is farther downwind. Results also indicate that larger portion of small storms (50–200 km^2) and large/merged storms (>1500 km^2) were downwind of the urban region, whereas midsized storms (200–1500 km^2) dominate the upwind region.

A case study on a 13 June 2005 storm was further examined using MM5. The CONTROL-simulation synoptic setup agreed with the observations. Despite the small area of convection, the model represented the event well, although the model was slower in the development and evolution of the storm. A model sensitivity test was conducted in which the actual urban region was replaced with the dominant land use around the urban region. The change in land use characteristics proved to change the event and boundary layer characteristics, and the convection location. Within the researched urban area, the model did not simulate convection. Also, boundary layer parameters such as vertical velocity and θ_v were considerably different between the two simulations. Prestorm environment analysis over the urban region showed that the urban region increased vertical velocity fields as well as boundary layer height. During the convective initiation window near 0000 UTC, the CONTROL and NOURBAN fields were also different from each other. The CONTROL run depicted much greater vertical velocities in the prestorm environment capable of breaking the existing boundary layer capping inversion, unlike the NOURBAN case. Although the urban region might not be causing these effects directly, these simulations show that removing the urban region altered atmospheric flow patterns significantly. Therefore, land/surface flow patterns are important to consider when studying the atmosphere in and around urban regions.

Overall, when compared with the same time periods for other rural regions, the Indianapolis urban region proved to alter observed storm cases. Large differences in urban–rural characteristics (enhanced because of LULC contrast and a lack of topographical features in this region) most likely lead to an increase in storm-composition change in the urban region. Additional

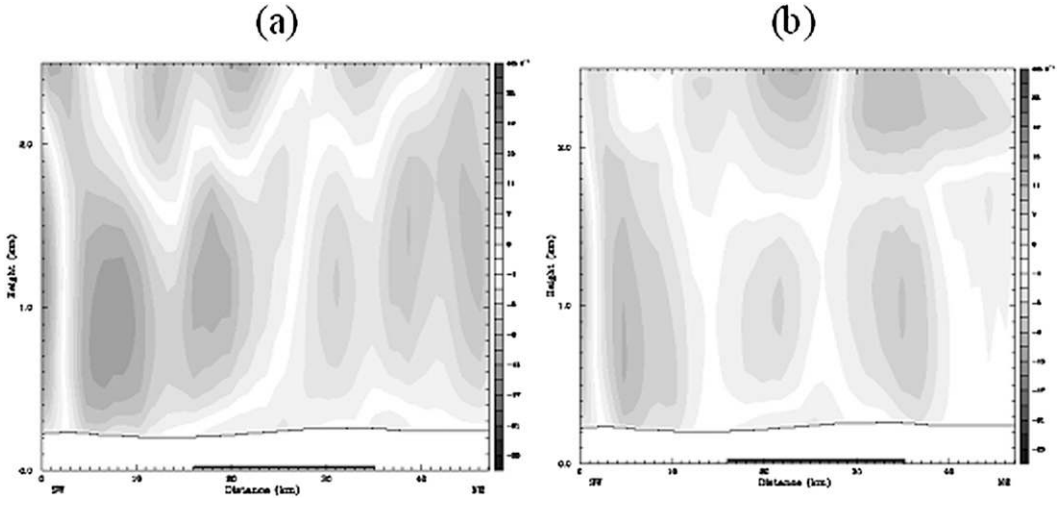

FIG. 16. (a) CONTROL and (b) NOURBAN C–D cross section (0–2.5 km) of vertical velocity on a scale from −25 to 25 cm s^{-1}. The Indianapolis urban region location is outlined in black along the x axis.

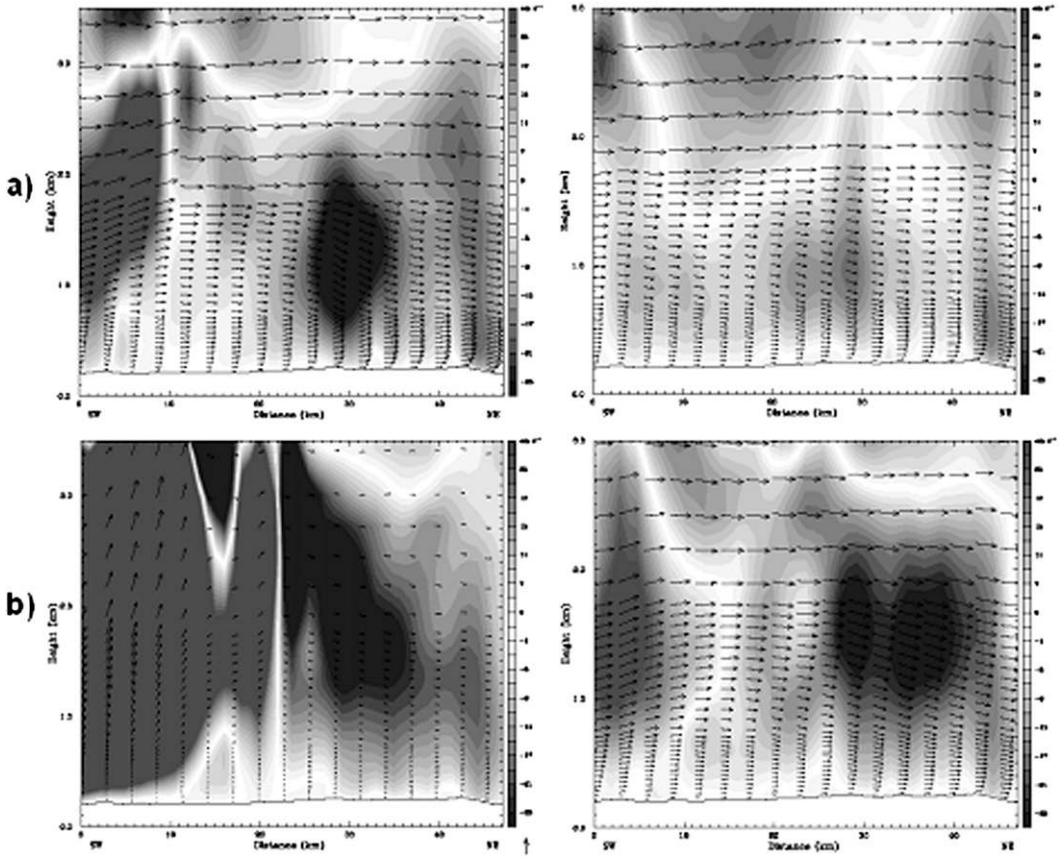

FIG. 17. Cross-sectional plot (0–2.5 km) from the southwestern portion of nest 4 (1.33 km) showing vertical velocities [shaded; gray (mostly in left of each panel) = positive and dark gray to black (mostly in center and right of each panel) = negative] and circulation vectors (vector arrows) for (a) 0000 and (b) 0030 UTC 14 Jun for (left) CONTROL and (right) NOURBAN cases.

observational analysis, including a suite of observations and much in-depth synoptic and mesoscale analysis, can contribute significantly to future urban climate studies. Modeling analysis for 13 June 2005 supported evidence of urban-influenced storm-composition change. Additional modeling for cases forced by varying synoptic conditions could lead to further information that could improve the modeling representation of urban areas as well as observational analysis for real-time forecasting. Overall results provide strong evidence that urban areas such as the Indianapolis region affect the regional climate by altering thunderstorm and rainfall patterns.

Acknowledgments. This study benefited in part through support from the U.S. DOE Atmospheric Radiation Measurement Program (DOE ARM 08ER64674; Dr. Rick Petty), NASA Terrestrial Hydrology Program (Drs. Jared Entin and Bhaskar Choudhury), National Science Foundation INTEROP program, NASA LCLUC (Dr. Garik Gutman), NASA Precipitation Measurement Missions program (Dr. Ramesh Kakar), and JCSDA/NOAA. We gratefully acknowledge many fruitful comments and suggestions from Prof. Julie Winkler and anonymous reviewers that helped to improve the presentation and the paper.

REFERENCES

Bentley, M. L., W. S. Ashley, and J. A. Stallins, 2010: Climatological radar delineation of urban convection for Atlanta, Georgia. *Int. J. Climatol.,* **30,** 1589–1594.

Bornstein, R. D., and Q. Lin, 2000: Urban heat islands and summer convective thunderstorms in Atlanta: Three case studies. *Atmos. Environ.,* **34,** 507–516.

Braham, R. R., Jr., 1981: Urban precipitation processes. *METROMEX: A Review and Summary, Meteor. Monogr.,* No. 40, Amer. Meteor. Soc., 75–116.

Changnon, S. A., Jr., 1968: The La Porte anomaly—fact or fiction? *Bull. Amer. Meteor. Soc.,* **49,** 4–11.

——, Ed., 1981: *METROMEX: A Review and Summary. Meteor. Monogr.,* No. 40, Amer. Meteor. Soc., 181 pp.

——, R. T. Shealy, and R. W. Scott, 1991: Precipitation changes in fall, winter, and spring caused by St. Louis. *J. Appl. Meteor.,* **30,** 126–134.

Chen, F., and J. Dudhia, 2001: Coupling an advanced land surface–hydrology model with the Penn State–NCAR MM5 modeling

system. Part I: Model implementation and sensitivity. *Mon. Wea. Rev.,* **129,** 569–585.

Cotton, W. R., and R. A. Pielke Sr., 2007: *Human Impacts on Weather and Climate*. Cambridge University Press, 330 pp.

Fall, S., D. Niyogi, R. A. Pielke Sr., A. Gluhovsky, E. Kalnay, and G. Rochon, 2009: Land use land cover impacts temperature trends over the continental United States: Assessment using the North American Regional Reanalysis. *Int. J. Climatol.,* **30,** 1980–1993.

Fujibe, F., and T. Asai, 1980: Some features of the surface wind system associated with the Tokyo heat island. *J. Meteor. Soc. Japan,* **58,** 149–152.

Gero, A. F., and A. J. Pitman, 2006: The impact of land cover change on a simulated storm event in the Sydney Basin. *J. Appl. Meteor. Climatol.,* **45,** 283–300.

——, ——, G. T. Narisma, C. Jacobsen, and R. A. Pielke Sr., 2006: The impact of land cover change on storms in the Sydney Basin. *Global Planet. Change,* **54,** 57–78.

Hafner, J., and S. Kidder, 1999: Urban heat island modeling in conjunction with satellite-derived surface/soil parameters. *J. Appl. Meteor.,* **38,** 448–465.

Hand, L., and J. M. Shepherd, 2009: An investigation of warm-season spatial rainfall variability in Oklahoma City: Possible linkages to urbanization and prevailing wind. *J. Appl. Meteor. Climatol.,* **48,** 251–269.

Hjelmfelt, M. R., 1982: Numerical simulation of the effects of St. Louis on mesoscale boundary-layer airflow and vertical motion: Simulations of urban vs non-urban effects. *J. Appl. Meteor.,* **21,** 1239–1257.

Holt, T., D. Niyogi, F. Chen, M. A. LeMone, K. Manning, and A. L. Qureshi, 2006: Effect of land–atmosphere interactions on the IHOP 24–25 May 2002 convection case. *Mon. Wea. Rev.,* **134,** 113–133.

Huff, F. A., 1986: Urban hydrological review. *Bull. Amer. Meteor. Soc.,* **67,** 703–712.

——, and S. A. Changnon Jr., 1972: Climatological assessment of urban effects on precipitation at St. Louis. *J. Appl. Meteor.,* **11,** 823–842.

Ikebuchi, S., K. Tanaka, Y. Ito, Q. Moteki, K. Souma, and K. Yorozu, 2007: Investigation of the effects of urban heating on the heavy rainfall event by a cloud resolving model CReSiBUC. *Ann. Disaster Prev. Res. Inst., Kyoto Univ.,* **50C,** 105–111.

Jauregui, E., and E. Romales, 1996: Urban effects on convective precipitation in Mexico City. *Atmos. Environ.,* **30,** 3383–3389.

Kain, J. S., 2004: The Kain–Fritsch convective parameterization: An update. *J. Appl. Meteor.,* **43,** 170–181.

Kishtawal, C., D. Niyogi, M. Tewari, R. A. Pielke Sr., and M. Shepherd, 2010: Urbanization signature in the observed heavy rainfall climatology over India. *Int. J. Climatol.,* **30,** 1908–1916.

Landsberg, H. E., 1970: Man-made climatic changes. *Science,* **170,** 1265–1274.

Lei, M., D. Niyogi, C. Kishtawal, R. Pielke Sr., A. Beltrán-Przekurat, T. Nobis, and S. Vaidya, 2008: Effect of explicit urban land surface representation on the simulation of the 26 July 2005 heavy rain event over Mumbai, India. *Atmos. Chem. Phys.,* **8,** 8773–8816.

Liu, Y., F. Chen, T. Warner, and J. Basara, 2006: Verification of a mesoscale data-assimilation and forecasting system for the Oklahoma City area during the Joint Urban 2003 Field Project. *J. Appl. Meteor. Climatol.,* **45,** 912–929.

Lo, J. C. F., A. K. H. Lau, F. Chen, J. C. H. Fung, and K. K. M. Leung, 2007: Urban modification in a mesoscale model and the effects on the local circulation in the Pearl River delta region. *J. Appl. Meteor. Climatol.,* **46,** 457–476.

Loose, T., and R. D. Bornstein, 1977: Observations of mesoscale effects on frontal movement through an urban area. *Mon. Wea. Rev.,* **105,** 563–571.

Miao, S., and F. Chen, 2008: Formation of horizontal convective rolls in urban areas. *Atmos. Res.,* **89,** 298–304.

Mote, T. L., M. C. Lacke, and J. M. Shepherd, 2007: Radar signatures of the urban effect on precipitation distribution: A case study for Atlanta, Georgia. *Geophys. Res. Lett.,* **34,** L20710, doi:10.1029/2007GL031903.

Niyogi, D., T. Holt, S. Zhong, P. C. Pyle, and J. Basara, 2006: Urban and land surface effects on the 30 July 2003 mesoscale convective system event observed in the southern Great Plains. *J. Geophys. Res.,* **111,** D19107, doi:10.1029/2005JD006746.

Oke, T., 1988: *Boundary Layer Climates*. Routledge, 464 pp.

Oliver, J., 2009: *Indiana's Weather and Climate*. Indiana University Press, 192 pp.

Pielke, R. A., and D. Niyogi, 2009: The role of landscape processes within the climate system. *Landform—Structure, Evolution, Process Control,* J. C. Otto and R. Dikau, Eds., Lecture Notes in Earth Sciences, Vol. 115, Springer, 67–86.

Reisner, J., R. M. Rasmussen, and R. T. Bruintjes, 1998: Explicit forecasting of supercooled liquid water in winter storms using the MM5 mesoscale model. *Quart. J. Roy. Meteor. Soc.,* **124,** 1071–1107.

Rose, S., J. A. Stallins, and M. Bentley, 2008: Climatological and single-event scale visualizations of urban cloud-to-ground flashes in Atlanta, Georgia. *Earth Interact.,* **12**. [Available online at http://earthinteractions.org/.]

Rozoff, C., W. R. Cotton, and J. O. Adegoke, 2003: Simulation of St. Louis, Missouri, land use impacts on thunderstorms. *J. Appl. Meteor.,* **42,** 716–738.

Shem, W., and M. Shepherd, 2009: On the impact of urbanization on summertime thunderstorms in Atlanta: Two numerical model case studies. *Atmos. Res.,* **92,** 172–189.

Shepherd, J. M., and S. J. Burian, 2003: Detection of urban induced rainfall anomalies in a major coastal city. *Earth Interact.,* **7**. [Available online at http://earthinteractions.org/.]

——, H. Pierce, and A. J. Negri, 2002: Rainfall modification by major urban areas: Observations from spaceborne rain radar on the TRMM satellite. *J. Appl. Meteor.,* **41,** 689–701.

——, W. M. Carter, M. Manyin, D. Messen, and S. Burian, 2010: The impact of urbanization on current and future coastal convection: A case study for Houston. *Environ. Plann.,* **37,** 284–304.

Shreffler, J. H., 1978: Detection of centripetal heat-island circulations from tower data in St. Louis. *Bound.-Layer Meteor.,* **15,** 229–242.

Thompson, W. T., T. Holt, and J. Pullen, 2007: Investigation of a sea breeze front in an urban environment. *Quart. J. Roy. Meteor. Soc.,* **133,** 579–594.

Zhang, C.-L., F. Chen, S.-G. Miao, Q.-C. Li, X.-A. Xia, and C.-Y. Xuan, 2009: Impacts of urban expansion and future green-planting on summer precipitation in the Beijing metropolitan area. *J. Geophys. Res.,* **114,** D02116, doi:10.1029/2008JD010328.

Zhou, L., R. E. Dickinson, Y. Tian, J. Fang, Q. Li, R. K. Kaufmann, C. J. Tucker, and R. B. Myneni, 2004: Evidence for a significant urbanization effect on climate in China. *Proc. Natl. Acad. Sci. USA,* **101,** 9540–9544.

Zhou, Y., and J. M. Shepherd, 2009: Atlanta's urban heat island under extreme heat conditions and potential mitigation strategies. *Nat. Hazards,* **52,** 639–668.